Examining the structural changes in $Fe_2(CO)_9$ under high external pressures by Raman spectroscopy[1]

Muhieddine Safa, Zhaohui Dong, Yang Song, and Yining Huang

Abstract: Pressure-induced structural changes in di-iron nonacarbonyl [$Fe_2(CO)_9$] were examined by in situ Raman spectroscopy with the aid of a diamond anvil cell. Our results indicate that $Fe_2(CO)_9$ undergoes a pressure-induced phase transformation at about 0.9 GPa. Upon further compression, another structural transformation is identified at 7 GPa. In the low-pressure phase below 0.9 GPa, the π back-bonding between metal and carbonyl increases with increasing pressure. In the high-pressure phase above 7 GPa, the combination of high-pressure and laser irradiation induces a change in structure from $Fe_2(CO)_9$ to $Fe_2(CO)_8$. $Fe_2(CO)_8$ appears to adopt a structure with C_{2v} rather than D_{3d} or D_{2h} symmetry. The metal–metal bond is gradually weakened under high pressures, and $Fe_2(CO)_8$ eventually decomposes by breaking the Fe–Fe bond when compressed up to 17.7 GPa.

Key words: metal carbonyl, Raman spectroscopy, high pressure, diamond anvil cell.

Résumé : Faisant appel à la spectroscopie Raman in situ avec l'aide d'une cellule à matrice de diamant, on a étudié les changements structuraux induits par la pression dans le difernonacarbonyle, [$Fe_2(CO)_9$]. Les résultats obtenus indiquent que le $Fe_2(CO)_9$ subit une transformation de phase induite par la pression à environ 0,9 GPa. Par compression subséquente, on a identifié une autre transformation structurale à 7 GPa. Dans la phase à basse pression, en dessous de 0,9 GPa, la liaison en retour π entre le métal et les carbonyles augmente avec une augmentation de pression. Dans la phase à haute pression, au-dessus de 7 GPa, une combinaison de pression élevée et une irradiation au laser induit un changement dans la structure de $Fe_2(CO)_9$ à $Fe_2(CO)_8$. Le $Fe_2(CO)_8$ semble adopter une structure de symétrie C_{2v} plutôt que les symétries D_{3d} ou D_{2h}. La liaison métal–métal s'affaiblit graduellement sous des pressions élevées et le $Fe_2(CO)_8$ se décompose éventuellement par bris de la liaison Fe–Fe lorsqu'on atteint une pression de 17,7 GPa.

Mots-clés : métal carbonyle, spectroscopie Raman, pression élevée, cellule à matrice de diamant.

[Traduit par la Rédaction]

Introduction

Vibrational spectroscopy has long been the method of choice for the characterization of organometallic compounds because it provides invaluable information on the molecular geometry, crystal structures of the solid complexes, and the nature of the bonding interactions in these compounds. Using external pressure as an independent variable to explore the change in molecular geometry and phase behavior of organometallic carbonyls is quite important, since many of the transition metal carbonyls exhibit interesting changes in both molecular and crystal structures under high external pressures (1, 2), but these changes often do not occur upon lowering temperatures.

The high-pressure studies are usually performed with the aid of diamond anvil cells (DACs). Coupling of a DAC to a Raman spectrometer provides an extremely useful approach to examine the metal carbonyls under pressures because the spectra in the CO stretching region (~2000 cm^{-1}) are very sensitive to the change of molecular geometry and crystal structure. The pressure dependences ($d\nu/dP$) of the ν(CO) and ν(M–CO) modes of transition-metal carbonyls provide the information regarding the π back-bonding between metals and the carbonyl groups. The corresponding IR spectroscopy is much less useful, since the strong diamond adsorption completely masks the ν(CO) region (3).

The structures of binuclear transition-metal carbonyls, such as $Mn_2(CO)_{10}$, $Re_2(CO)_{10}$ and $MnRe(CO)_{10}$ have been examined by Raman spectroscopy under high pressures (4, 5). A second-order phase transition was detected, but more interestingly, the molecular geometry changed from the staggered structure (D_{4d}) to an eclipsed configuration (D_{4h}) in each case.

Tri-μ-carbonyl(hexacarbonyl)di-iron(0), $Fe_2(CO)_9$, was one of the earliest known metal carbonyls and remains to be one of the best-known examples for binuclear transition-metal carbonyls. This complex is an important reagent for organic synthesis and is a catalyst as well. The crystal struc-

Received 09 May 2007. Accepted 30 June 2007. Published on the NRC Research Press Web site at canjchem.nrc.ca on 21 September 2007.

This manuscript is dedicated to Professor G. Mike Bancroft in honor of his 65th birthday.

M. Safa, Z. Dong, Y. Song,[2] and Y. Huang.[3] Department of Chemistry, The University of Western Ontario, London, ON N6A 5B7, Canada.

[1]This article is part of a Special Issue dedicated to Professor G. Michael Bancroft.

[2]Corresponding author (e-mail: yang.song@uwo.ca).
[3]Corresponding author (e-mail: yhuang@uwo.ca)

 doi:10.1139/V07-096

ture has been determined by single-crystal X-ray diffraction (6, 7). The unit cell adopts a space group of $P6_3/m$ with two molecules per unit cell residing at C_{3h} sites and a molecular symmetry of D_{3h} (Fig. 1). The vibrational spectra of $Fe_2(CO)_9$ at ambient pressure and low temperature have been assigned (8–10). The low-temperature Raman studies indicated that there is no phase transition occurring at temperatures as low as 15 K (8). In addition, $Fe_2(CO)_9$ exhibits interesting photochemistry. The early study of Poliakoff and Turner showed that this complex undergoes the CO disassociation under irradiation (11, 12). $Fe_2(CO)_8$ was captured as a key product at very low temperature in matrixes. Structures of di-iron carbonyls with different stoichiometry [$Fe_2(CO)_x$] together with their bonding natures between the two irons have been extensively characterized by Xie et al. (13) using various computational approaches. Very recently, the photochemistry of $Fe_2(CO)_9$ was further examined by Bertini et al. (14) using time-dependent DFT theory.

In the present study, we have investigated the behavior of $Fe_2(CO)_9$ under high external pressures up to about 18 GPa. Particular attention was paid to the possible pressure-induced phase transition, the geometry change and the combining effect of laser irradiation and applying high pressure on the photochemical behavior of $Fe_2(CO)_9$.

Experimental

Polycrystalline powder of $Fe_2(CO)_9$ was purchased from Alfa Aesar Chemical Company (purity ≥99%) and was used without further purification. Raman spectra were recorded on a Renishaw Model 2000 Raman spectrometer equipped with a Leica microscope and a thermoelectronically cooled CCD detector. The 632.8 nm line of a HeNe laser was used as the excitation source with an average power of several milliwatts at the sample. The resolution achieved was typically 1 cm^{-1}. The sample and several tiny ruby chips were placed in a stainless steel gasket (250 μm in diameter and 70 μm thick) mounted between two opposing anvils of a symmetric piston-cylinder type DAC. The DAC was then mounted onto an X–Y stage, and the laser beam was focused on the sample via a 4X microscope objective. The pressure was calibrated by using the well-known ruby method (15). No pressure media were used. The uncertainty for pressure determination is estimated as 0.05 GPa.

Results

Raman spectra of $Fe_2(CO)_9$ at 0–7 GPa

The Raman spectrum of $Fe_2(CO)_9$ was collected at ambient pressure and room temperature before compression and is depicted in Fig. 2. The structure of $Fe_2(CO)_9$ at ambient pressure has been well-established and extensively characterized by X-ray diffraction and vibrational spectroscopy. Under factor group analysis (9), 18 modes are predicted to be Raman active and eight modes to be IR active, while 10 modes are both Raman and IR active out of a total of 54 vibrational modes. In general, the Raman active modes are observed in two spectral regions, i.e., 1800–2150 cm^{-1} and below 600 cm^{-1}, corresponding to the carbonyl stretching and iron–carbonyl cluster vibrations, respectively. Our Raman spectrum is consistent with previous vibrational studies (9) with the major characteristic modes being observed. The assignments of these modes are labeled in Fig. 2 and listed in Table 1 in comparison with previous observations. In the carbonyl stretching region, the peaks at 2107, 2013, and 1988 cm^{-1} are attributed to the terminal carbonyls

Fig. 1. Molecular structure of $Fe_2(CO)_9$.

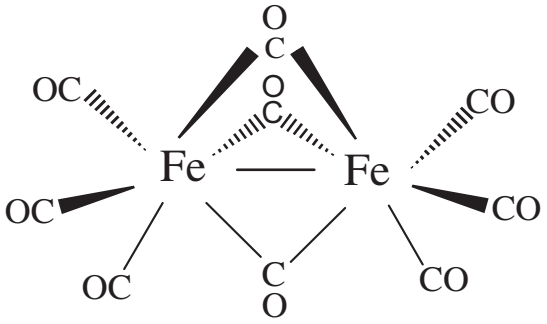

Fig. 2. Selective Raman spectra of $Fe_2(CO)_9$ on compression at 0–5.8 GPa in the spectral regions of 100–650 cm^{-1} and 1800–2150 cm^{-1}. The pressures in GPa are labeled for each spectrum. The assignments of the Raman modes are labeled on the top spectrum collected at ambient pressure. The spectra are normalized to the same scale and offset vertically for clarity.

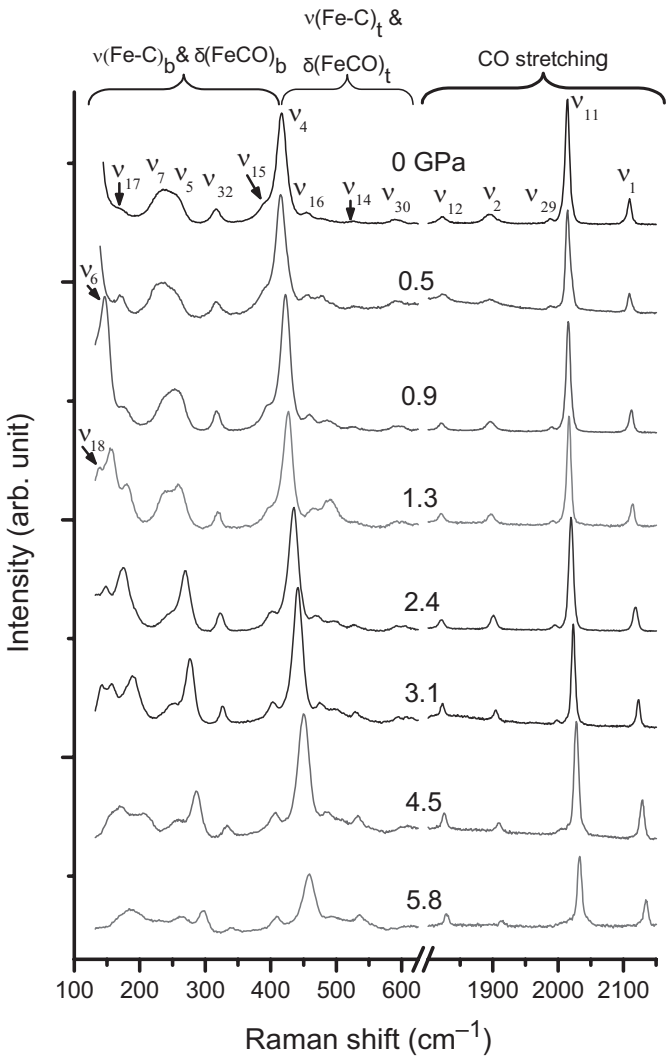

Table 1. Assignment of Raman active modes of solid $Fe_2(CO)_9$ observed at ambient pressure and room temperature.

Mode	This work (cm^{-1})	Reference 8 (cm^{-1})	Description[a]
ν_1 (A_g)	2107	2112	$\nu(CO)_t$
ν_{11} (E_{2g})	2013	2016	
ν_{29} (E_{1g})	1988	1990	
ν_2 (A_g)	1895	1891	$\nu(CO)_b$
ν_{12} (E_{2g})	1824	1814	
ν_{30} (E″)	594	590	$(Fe–CO)_t$
ν_{14} (E′)	529	528	$\delta(Fe–CO)_t$
ν_{31} (E″)	494	493	
ν_3 (A′)	480	480	
ν_{16} (E′)	457	451	$\nu(Fe–C)_t$
ν_4 (A'_1)	415	415	
ν_{15} (E′)	393	390	$\delta(Fe–CO)_b$
ν_{32} (E″)	316	315	
ν_5 (A′)	248	260	$\nu(Fe–Fe)$, $\nu(Fe–C)_b$
ν_7 (A′)	236	237	
ν_{17} (E′)	171	175	$\nu(Fe–C)_b$
ν_6 (A'_1)[b]	142	137	$\delta(C–Fe–C)$, $\Delta(Fe_2C_3)$
ν_{18} (E′)[c]	138	126	

[a]ν: Stretching; δ: bending; Δ: cluster vibration; t: terminal; and b: bridging.
[b]First observed at 0.9 GPa.
[c]First observed at 1.3 GPa

$[\nu(CO)_t]$, while those at 1895 and 1824 cm^{-1} are associated with bridging carbonyls $[\nu(CO)_b]$. In the spectral region between 600 and 400 cm^{-1}, the vibrations are associated with the bending of the terminal carbonyls $[\delta(Fe–CO)_t]$ and the stretching between iron and terminal carbonyls $[\nu(Fe–C)_t]$. The modes below 400 cm^{-1} are due to the bending of bridging carbonyls $[\delta(Fe–CO)_b]$, the stretching between iron and bridging carbons $[\nu(Fe–C)_b]$, as well as some vibrations from iron-centred cluster $[\Delta Fe_2C_3]$ (9).

Upon compression, the Raman modes for carbonyl stretching shift to higher frequencies smoothly. The Raman intensities of these modes are relatively insensitive to pressure except for mode ν_{29}, a $\nu(CO)_t$ mode, the intensity of which decreases with pressure significantly. In the lower vibrational frequency region, the major Raman modes are found to shift to higher frequencies markedly. In addition, significant changes in Raman patterns are found in this region. For instance, ν_{15}, a very weak $\delta(FeCO)_b$ mode at 393 cm^{-1} at ambient pressure, becomes a resolvable shoulder of ν_4 mode at 0.9 GPa and is completely deconvoluted from ν_4 mode at 5.8 GPa. Furthermore, the ν_7 and ν_5 modes, which exhibit a broad convoluted peak at ambient pressure, become a resolvable doublet at 1.3 GPa, which further develops into two bands with strongly constrasting intensities. The most drastic changes of the Raman spectra are observed below 200 cm^{-1}. The ν_{17} mode is greatly enhanced by compression between 0.5–1.3 GPa but becomes indiscernible beyond 1.3 GPa. More interestingly, a new Raman mode, which is identified as ν_6 (Table 1), is observed at 0.9 GPa. This mode, which is not observable at lower pressures because of the use of an edge filter in the Raman spectrometer, shifts rapidly to higher frequency until 5.8 GPa when the intensity drops significantly. Other new modes observed include the ν_{18} mode at 138 cm^{-1} at 1.3 GPa and a band at 142 cm^{-1} at 3.1 GPa, which can be assigned as a mode associated with the iron-centred cluster vibration. These low-frequency modes become very weak with increasing pressure up to 5.8 GPa.

Raman spectra of $Fe_2(CO)_9$ at 7–17.7 GPa

Raman spectra of $Fe_2(CO)_9$ at 7–17.7 GPa are depicted in Fig. 3. At 7 GPa, eight Raman modes (ν_{18}, ν_7, ν_5, ν_{32}, ν_{15}, ν_4, ν_{16}, and ν_{14}) are observed in the low-wavenumber region below 600 cm^{-1}. These modes shift to higher wavenumbers with pressure, and their intensities decrease systematically. Concurrent to the weakening of Raman intensities, all bands become significantly broader with only three bands (ν_5, ν_4, and ν_{14}) identifiable at 12.3 GPa. When pressure is increased to 17.7 GPa, the Raman features in this region completely disappeared, indicating the destruction of the Fe–C cluster. The most striking change is observed in the carbonyl stretching region. A new peak at 2018 cm^{-1} is observed at 7.0 GPa, which develops into a relatively intense Raman mode with increasing pressure. When pressure is increased to 9.7 GPa, another new peak at 2056 cm^{-1} was observed all the way to 12.3 GPa. The intensities of these carbonyl stretching modes

Fig. 3. Selective Raman spectra of $Fe_2(CO)_9$ on compression at 7.0–17.7 GPa in the spectral regions 100–650 cm^{-1} and 1800–2200 cm^{-1}. The pressures in GPa are labeled for each spectrum. The assignments of the Raman modes are labeled on the top spectrum collected at 7.0 GPa. The spectra are normalized to the same scale and offset vertically for clarity.

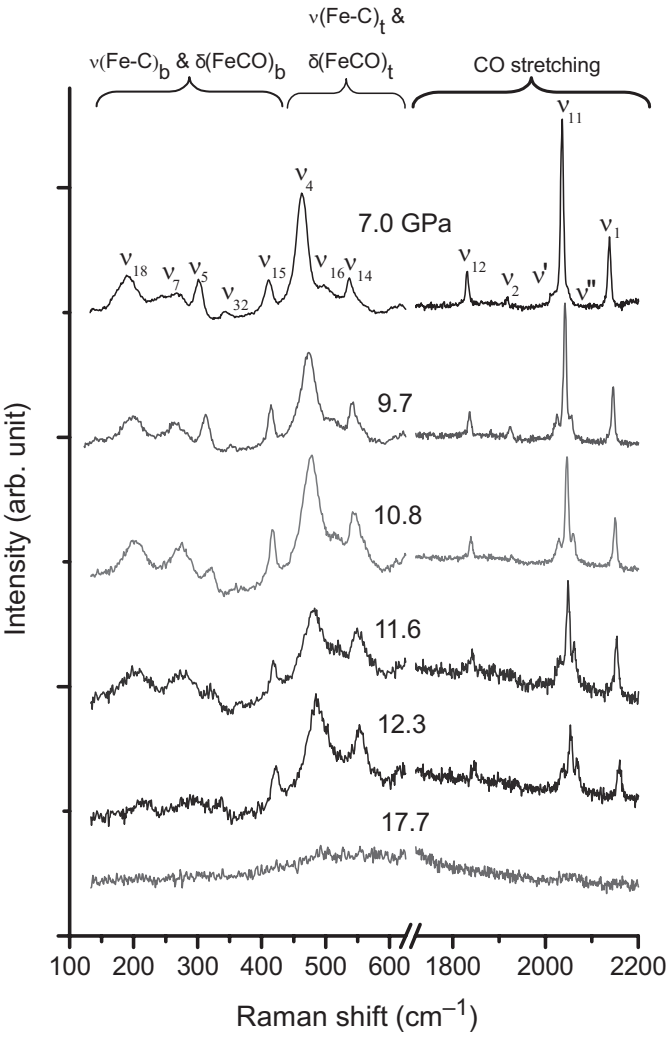

are also reduced by compression with the ν_2 mode being completely unobservable at 11.6 GPa. Similar to the low frequency regions, the carbonyl stretching region exhibits absolutely no Raman feature at 17.7 GPa, indicating the compound has completely decomposed.

Pressure dependence of Raman modes of $Fe_2(CO)_9$

Figure 4 shows the Raman shifts of major modes in both the low-frequency region and the carbonyl stretching region as a function of pressure on compression. The pressure dependences $d\nu/dP$ are also listed in Table 2. As can be seen from the Fig. 4 and Table 2, below 0.9 GPa, all modes exhibit a positive linear dependence with pressure except for two modes, ν_{14} and ν_{12}, which have negative $d\nu/dP$ values. A distinct change in slope at 0.9 GPa is observed for almost all modes. In the region below 0.9 GPa, all modes follow a linear pressure dependence with larger $d\nu/dP$ values than those between 0.9 and 7 GPa, except for ν_{16}, ν_2, and ν_{11} modes, which exhibit larger $d\nu/dP$ values at the higher pressure region. Most significantly, the ν_{29}, ν_{16}, and ν_{32} modes are not observed beyond 7 GPa, while new modes in the carbonyl stretching region are observed above 7 GPa (Fig. 3), indicating a major phase or structural transition.

Discussion

Figure 4 illustrates that in the pressure region below 7 GPa, most of the Raman modes exhibit a distinct break in the slopes of the $\nu - P$ plots at around 0.9 GPa, suggesting that there is a pressure-induced phase transition. Since the discontinuities in Fig. 4 are not abrupt, and there is no change in the number of internal modes at the transition, the observed phase transformation is likely second-order. Previous vibrational studies showed no phase change occurring at low-temperature (8). Therefore, the new phase appears to only exist under high pressures.

In the low-pressure phase, three high-frequency bands at 2107, 2013, and 1988 cm^{-1} due to the terminal carbonyl stretching vibrations [$\nu(CO)_t$] steadily shifted to higher frequencies with increasing pressure. The band at 1895 cm^{-1} is almost pressure-insensitive, while the 1824 cm^{-1} band has a negative pressure-shift rate, i.e., it shifts to lower frequencies with increasing pressure. Both the 1895 and 1824 cm^{-1} bands are due to the bridging carbonyl stretching modes, [$\nu(CO)_b$]. Normally, all the internal modes shift gradually with increasing external pressure because of the anharmonicity of the potential function. Any unusual pressure behavior, such as very large, small, and even negative pressure dependence should be explained in terms of specific intra- and intermolecular interactions. The insensitivities and (or) negative pressure dependences of terminal $\nu(CO)_t$ modes have been reported in the previous high-pressure Raman studies on transition metal carbonyl complexes (16–18). Such observations were interpreted as the pressure-enhanced π back-bonding between the metal centre and the CO groups, i.e., the strengthening of the π back-bonding decreases the carbonyl bond order, which results in a constant or decreasing $\nu(CO)$ frequency. In the present case, the two bridging $\nu(CO)_b$ modes exhibit a very small and a negative pressure dependence, suggesting that in the low-pressure phase, the π back-bonding between iron and bridging carbonyl groups is particularly enhanced under external pressure. It is also worth noting that the broad peak centred at around 260 cm^{-1} exhibits a very prominent positive pressure dependence (41.5 cm^{-1}/GPa) in the low-pressure phase. This band has been previously assigned to the Fe–Fe stretching mode (8, 9). Thus, the very large pressure shift rate of the ν(Fe–Fe) mode implies that the metal–metal bond is significantly shortened by pressure.

All the results indicate that in the low-pressure phase, increasing pressure significantly affects the cluster involving two metal centres and three bridging CO groups [$(Fe_2C_3)_b$]. It appears that the bonding interactions responsible for holding the cluster together, such as metal–metal bond and the bonding between bridging CO and metal centres, are strengthened by pressure. Several binuclear transition-metal carbonyl complexes, such as $Mn_2(CO)_{10}$, $Re_2(CO)_{10}$, and $MnRe(CO)_{10}$, have been examined under high external pres-

Fig. 4. Raman shift of $Fe_2(CO)_9$ with pressure on compression for vibrations involving (*a*) iron–carbonyl and (*b*) bridging and terminal carbonyls. Different symbols denote Raman modes with different origins. The solid lines crossing the solid symbols are linear fit for eye guidance. The vertical dotted lines denote the proposed transition boundary. The assignments are labeled for each Raman active mode.

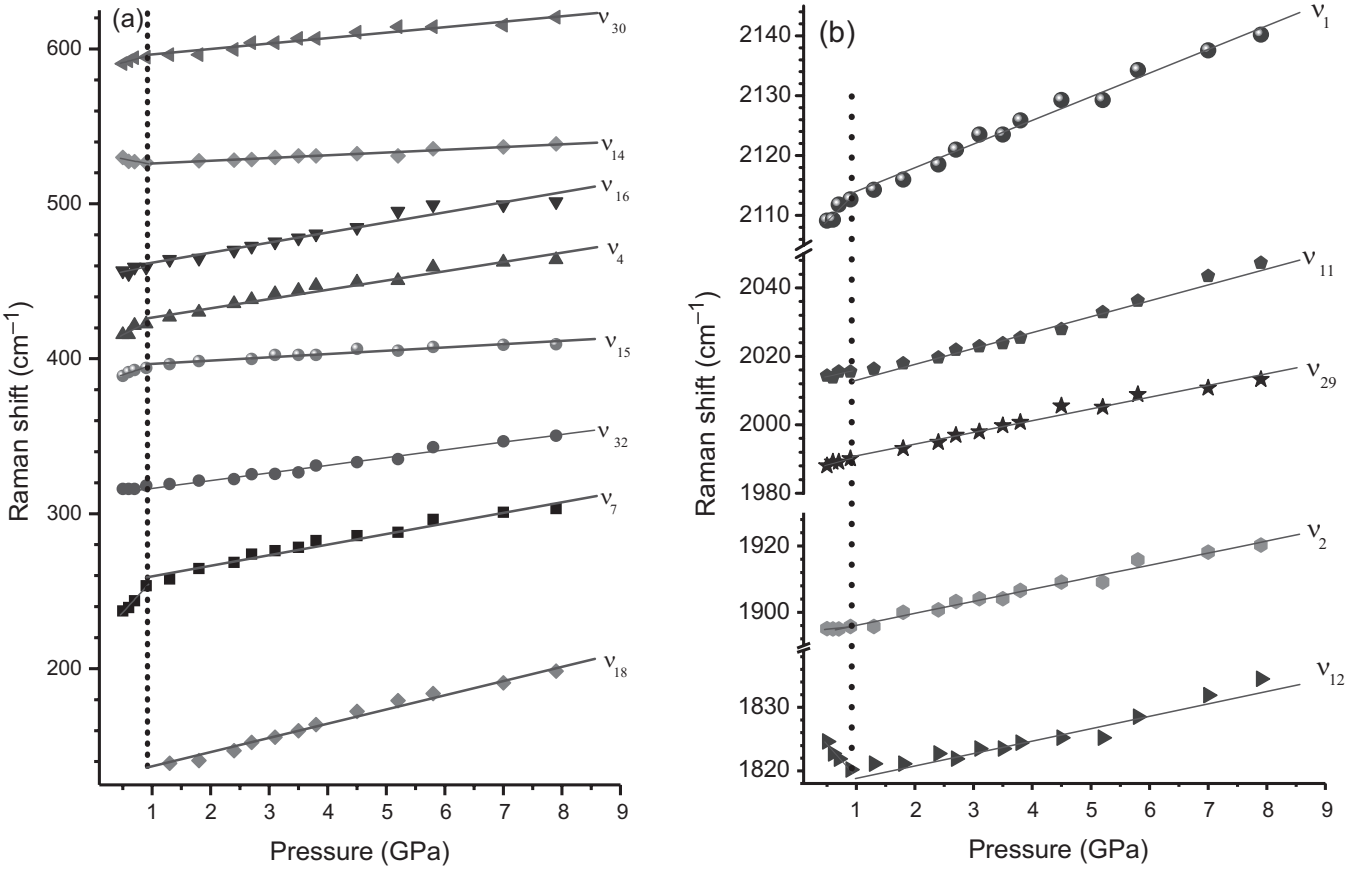

Table 2. Pressure dependence of Raman modes of $Fe_2(CO)_9$ at 0–7.0 GPa.

		$(d\nu/dP)_T$ (cm^{-1}/GPa)	
Raman modes	Frequency at ambient P (cm^{-1})	0–0.9 GPa	0.9–7.0 GPa
ν_{18}	138	—	10.7
ν_7	236	41.5	7.4
ν_{32}	316	5.5	5.0
ν_{15}	393	12.4	2.2
ν_4	415	19.4	6.3
ν_{16}	457	7.9	8.1
ν_{14}	529	–7.1	1.7
ν_{30}	594	10.3	3.8
ν_{12}	1824	–10.5	1.8
ν_2	1895	1.9	3.7
ν_{29}	1988	4.8	3.6
ν_{11}	2013	3.9	4.7
ν_1	2107	9.9	4.2

sure by Raman spectroscopy (4, 5). In each case, a change in molecular geometry from staggered (D_{4d}) to eclipsed (D_{4h}) configuration was observed. However, in the present case, the molecular geometry of $Fe_2(CO)_9$ remained as D_{3h}. Apparently, the pressure-strengthened interactions between metal centres and bridging carbonyl groups via π bonding prevents any rotation of $Fe(CO)_3$ fragment around Fe–Fe axis from changing to other configurations.

In the high-pressure phase (0.9–5.8 GPa), all the ν(CO) stretching modes are gradually shifting to the higher frequencies, including the two bands due to the bridging carbonyl groups. Overall, there is no major change in the appearance of the spectra in the ν(CO) region, indicating no change in the molecular geometry in this high-pressure phase. As shown in Fig. 2, in the low-frequency region, all the bands originating from the $(Fe_2C_3)_b$ cluster as well as all the $(Fe–CO)_b$ stretching and bending vibrations are gradually broadened with increasing pressure except for the ν_7 mode, which is mainly due to metal–metal bonding. All these results suggest that in the pressure range of 0.9–5.8 GPa, the $(Fe_2C_3)_b$ core is significantly distorted under pressure, while the $Fe(CO)_3$ groups involving terminal carbonyls are relatively unaffected.

When the pressure was increased to 7 GPa, some distinct changes were observed in the ν(CO) region. In particular, two new bands appeared at 2018 and 2056 cm^{-1} (Fig. 3). The appearance of these new bands in the ν(CO) region implies the formation of a new carbonyl species. The early work by Fletcher et al. showed that irradiation of $Fe_2(CO)_9$

Fig. 5. Proposed structures of $Fe_2(CO)_8$ with (*a*) D_{3d}, (*b*) D_{2h}, and (*c*) C_{2v} symmetries.

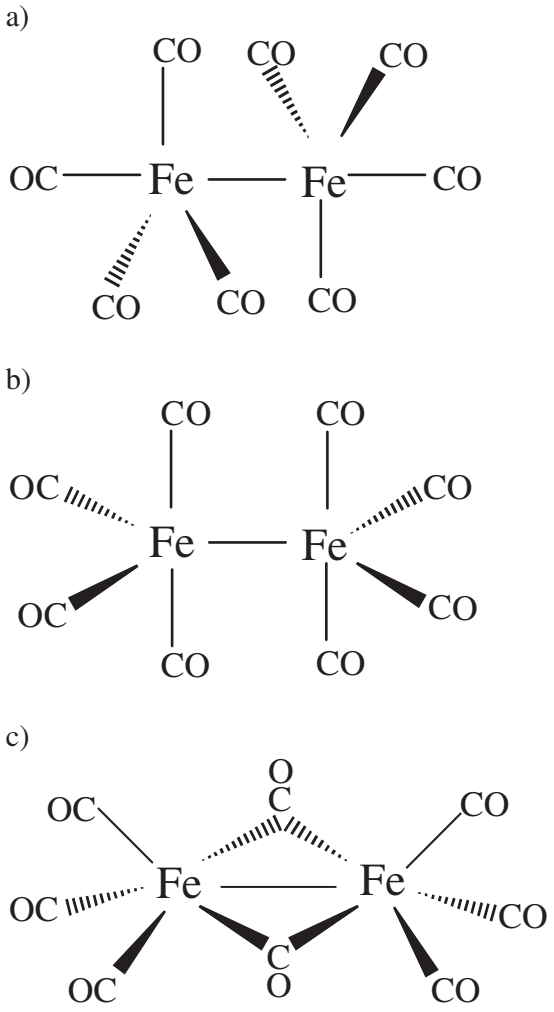

with UV light leads to the formation of $Fe_2(CO)_8$ at low temperature according to the following (11):

$$Fe_2(CO)_9 \rightarrow Fe_2(CO)_8 + CO$$

They were able to capture two $Fe_2(CO)_8$ isomers in matrices at 20 K: the CO bridged and unbridged $Fe_2(CO)_8$. The CO bridged isomer is a kinetic product and the unbridged compound is thermodynamically much more stable. The point groups of C_{2v} and D_{3d} were proposed for the CO bridged and unbridged $Fe_2(CO)_8$ species, respectively. The authors later established that the unbridged compound actually has D_{2h} symmetry (12). These symmetries are depicted in Fig. 5.

The work by Butler and co-workers showed that photolysis of $Fe_2(CO)_9$ can also occur during the acquisition of Raman spectra (8). In the present study, the appearance of additional ν(CO) bands suggest that $Fe_2(CO)_8$ is also formed by laser irradiation and stabilized by high external pressure. In particular, the frequencies of these new bands (2018 and 2056 cm^{-1}) are closer to those observed in the bridged $Fe_2(CO)_8$ (2022 and 2055 cm^{-1}) rather than the two high-frequency peaks of the unabridged isomer at 2006 and 2038 cm^{-1} (11). Therefore, the observations of five terminal $\nu(CO)_t$ and two bridging $\nu(CO)_b$ bands are consistent with C_{2v} symmetry (19). We also noticed that the intensity of the $\nu(CO)_b$ band, initially observed at 1895 cm^{-1}, quickly decreased with increasing pressure and is almost depleted completely at 12.6 GPa. It appears that $Fe_2(CO)_8$ may undergo further decomposition by losing one of the two bridging carbonyl groups.

In the low-frequency region, starting from 5.8 GPa, all the vibrations associated with $(Fe_2C_3)_b$ core, including the ν_7(Fe–Fe) mode, become gradually broadened with increasing pressure. At 12.3 GPa, all the previously mentioned bands become extremely broad. All these results suggest that the decomposition begins by breaking the $(Fe_2C_3)_b$ core, while the $Fe(CO)_3$ terminal groups are relatively unaffected in the beginning. Although peak broadening could be induced by structural amorphization or pressure gradients, the irreversible transformation and reasonably sharp ruby profiles rule out these possibilities and suggest that the transformation is chemical in nature. At 17.7 GPa, no Raman bands were observed, indicating that all the metal carbonyl species have completely decomposed.

Conclusions

In the present work, we have examined the behavior of $Fe_2(CO)_9$ under high external pressures. In the low-pressure range of 0–0.9 GPa, the pressure enhances the π back-bonding between the bridging CO ligands and the metal centres. The bonding interactions involving $(Fe_2C_3)_b$ cluster were strengthened upon compression in this pressure range. In the intermediate pressure region of 0.9–7 GPa, the molecular geometry remains as D_{3h}, but the $(Fe_2C_3)_b$ core undergoes distortion with increasing pressure. Above 7 GPa, gradual decomposition induced by the combination of pressure and laser irritation starts to be observed. $Fe_2(CO)_8$ with C_{2v} symmetry was identified as a product. This species at ambient pressure is very unstable and can only be captured at very low temperature in matrices. Apparently, this CO bridged compound is stabilized by high pressure. At higher pressure, further decomposition of $Fe_2(CO)_8$ was detected through losing a bridging CO group.

Acknowledgements

The authors are grateful to M.J. Walzak at Surface Science Western for her assistance with the Raman instrumentation. This work is supported by the Discovery Grants from Natural Sciences and Engineering Research Council of Canada (NSERC) and Academic Development Fund from The University of Western Ontario.

References

1. J.R. Ferraro. Vibrational spectroscopy at high external pressures: the diamond anvil cell. Academic Press, New York – Toronto. 1984.
2. C.M. Edwards and I.S. Butler. Coord. Chem. Rev. **199**, 1 (2000).
3. Z.X. Liu, J.Xu, H.P. Scott, Q. Williams, H.K. Mao, and R.J. Hemley. Rev. Sci. Instrum. **75**, 5026 (2004).
4. D.M. Adams, P.D. Hatton, A.C. Shaw, and T.K. Tan. J. Chem. Soc., Chem. Commun. **5**, 226 (1981).

5. D.M. Adams and I.O.C. Ekejiuba. J. Chem. Phys. **78**, 5408 (1983).
6. H.M. Powell and R.V.G. Ewens. J. Chem. Soc. 286 (1939).
7. F.A. Cotton and J.M. Troup. J. Chem. Soc., Dalton Trans. 800 (1974).
8. I.S. Butler, S. Kishner, and K.R. Plowman. J. Mol. Struct. **43**, 9 (1978).
9. D.M. Adams and I.D. Taylor. J. Chem. Soc., Faraday Trans. **78**, 1551 (1982).
10. S. Onaka and D.F. Shriver. Inorg. Chem. **15**, 915 (1976).
11. J.J. Turner and M. Poliakoff. J. Chem. Soc. A **4**, 654 (1971).
12. S.C. Fletcher, M. Poliakoff, and J.J. Turner. Inorg. Chem. **25**, 3597 (1986).
13. Y. Xie, H.F. Schaefer, and R.B. King. J. Am. Chem. Soc. **122**, 8746 (2000).
14. L. Bertini, C. Greco, L. De Gioia, and P. Fantucci. J. Phys. Chem. A **110**, 12900 (2006).
15. H.K. Mao, J. Xu, and P.M. Bell. J. Geophys. Res. **91**, 4673 (1986).
16. D.M. Adams and I.O.C. Ekejiuba. J. Chem. Phys. **77**, 4793 (1982).
17. Y. Huang, I.S. Butler, D.F.R. Gilson, and D. Lafleur. Inorg. Chem. **30**, 117 (1991).
18. Y. Huang, I.S. Butler, and D.F.R. Gilson. Inorg. Chem. **30**, 1098 (1991).
19. S.H.R. Brienne, R.D. Markwell, S.M. Barnett, I.S. Butler, and J.A. Finch. Appl. Spectrosc. **47**, 1131 (1993).